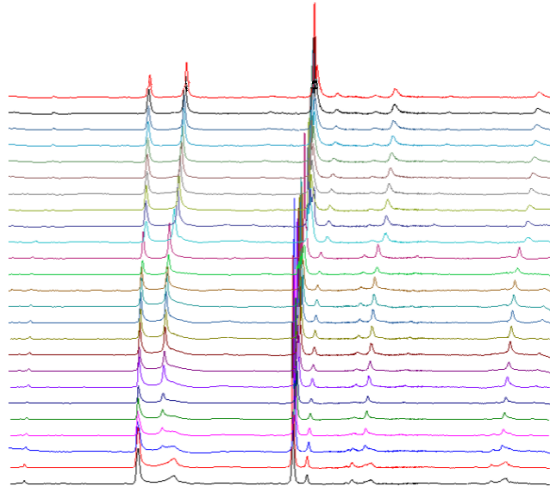


---

# Structure in Exotic Antiferromagnets

---



THESIS

submitted in partial fulfillment of the  
requirements for the degree of

MASTER OF SCIENCE  
in  
PHYSICS

Author :	Erik de Vos
Student ID :	1430750
Supervisor :	Jan van Ruitenbeek
2 <sup>nd</sup> corrector :	Siddharth Saxena

Cambridge, United Kingdom, March 27, 2018



# Structure in Exotic Antiferromagnets

**Erik de Vos**

Huygens-Kamerlingh Onnes Laboratory, Leiden University  
P.O. Box 9500, 2300 RA Leiden, The Netherlands

March 27, 2018

## **Abstract**

In this thesis research is presented into multiple unexplained phase transitions of the two antiferromagnets  $FePS_3$  and  $Fe_{1-x}S$  (pyrrhotite). X-ray diffraction and resistivity measurements of pressurised  $FePS_3$  show that this material undergoes at least two crystallographic phase transitions, strongly related to the appearance of an exotic metallic state when pressures over approximately 10GPa are applied. Magnetisation, specific heat and resistivity measurements of Pyrrhotite highlight for the first time the dual nature of the Besnus transition. Compelling evidence is presented that excludes the proposition of extrinsic magnetic coupling between differently ordered vacancy superstructures as the underlying mechanism. Instead the presence of local magnetic domain formation is highlighted.



# Contents

<b>1</b>	<b>Introduction</b>	<b>1</b>
<b>2</b>	<b>FePS<sub>3</sub></b>	<b>3</b>
<b>3</b>	<b>Pyrrhotite</b>	<b>17</b>
<b>4</b>	<b>Summary &amp; Outlook</b>	<b>27</b>



# Chapter 1

## Introduction

When one is introduced in the field that is broadly labelled as ‘Quantum Matter’, it often feels as if everything is known but very little is understood. This is inherently linked to the fact that all states of matter that we can classify as such are by definition emergent phenomena. But unlike many other emergent (soft & biological matter) physics, these states are intrinsically quantum mechanical, superconductivity being a well-known example. Fundamentally *we know* all the quantum mechanical rules governing the interactions between the electrons and the nuclei of our system. We *know* that the hamiltonian that fully describes this system is simply a superposition of the fundamental kinetic and (coulomb) potential hamiltonian of the electrons and nuclei and their corresponding coulomb interaction hamiltonian. However, the enormous amount of atoms in any type of condensed matter makes it virtually impossible to make any real predictions from this fact. This is why we build models, starting at the basic tight binding and free electron approximations and ending at far more complex density functional theory. These models help us *understand* more about the nature of these emergent phenomena and allow us to predict and describe their behavior.

Not only do new models such as these have to be tested, but quite often new materials are found that don’t seem to adhere to any of the known theoretical models. Experiments have to be conducted in order to obtain more information about their behavior. These experiments can then form the basis for future models. This means that the nature of emergent phenomena research is very experimentally oriented.

The nature of *quantum* emergent phenomena means that usually the limits of experimental conditions have to be approached in order to obtain new information. In practice this often encompasses going to very

low temperatures, high pressures and/or high magnetic fields. This thesis will describe several experiments performed at the Quantum Matter group at the Cavendish Laboratory in Cambridge. This group is one of the most knowledgeable about and has some of the best facilities for low-temperature and high pressure physics in the world. It will be referred to as 'the group' throughout this thesis.

In this thesis two ongoing researches into the materials  $FePS_3$  and  $Fe_{1-x}S$  (pyrrhotite) will be presented. Both of these materials show behavior that either does not fit to currently known models or is yet to be described by them. Focus will be primarily on resistivity, magnetisation and X-ray diffraction measurements, but temperature dependency of specific heat will also be discussed. One chapter is devoted to each of these materials. The results are summarized in the final chapter and an outlook on ongoing and possible further experimental investigations is given.

Experimental limits are rarely pushed in the research presented in this thesis. The characteristics of both pyrrhotite and  $FePS_3$  change remarkably at temperatures far above absolute zero and at pressures easily within experimental range. These materials are two prime examples of the fact that - even though the facilities are available - it isn't always necessary to go to the extremes of what is possible. Because in the end, all we have to *know* is that we want to *understand*. This thesis aims to do just that.

FePS<sub>3</sub>

*FePS<sub>3</sub>* is an ideal example of a low-temperature 2D antiferromagnetic insulator that can be tuned with pressure into an exotic metallic state. The emergence of these kinds of new states of matter from strongly correlated electron systems has been of interest in condensed matter physics for decades [2]. One famous area under investigation is unconventional superconductivity, which is a phase that often borders an insulating antiferromagnetic ground state. An example is depicted in the phase diagram in figure 2.1. Materials that exhibit this characteristic are often found to be quasi two-dimensional crystals [3]. This is explained via theoretical calculations by Monthoux and Lonzarich [4].

They showed that the superconducting transition temperature increases when the structure of a material becomes more and more two dimensional (moving from cubic to tetragonal and eventually towards two dimensionality). It was also found that the strength of the superconducting pairing interaction is enhanced by the proximity of an antiferromagnetic phase.

Unfortunately, the emergence of high-temperature superconductivity

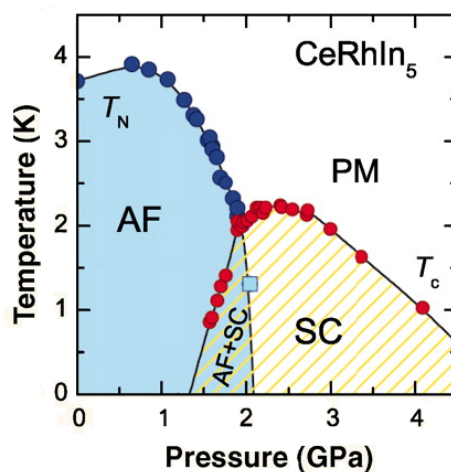


**Figure 2.1:** Phase diagram of *CeRhIn<sub>5</sub>*; a superconducting ‘dome’ can be seen to emerge from an insulating antiferromagnetic state when pressure is increased. Adapted from [1]

in a sense prevents the underlying ground state from being studied. In this case simpler models have to be sought in order to understand the tuning of this ground state towards unconventional metallic phases at higher temperatures. Materials from the  $MPX_3$  family (where  $M = \text{Fe, Ni, Mn}$  or other first-row divalent transition metals and  $X = \text{S, Se}$ ) are candidate materials for these model systems. They are layered two-dimensional insulators and exhibit a variety of interesting magnetic and electronic properties across the family, even though all the members of this family have approximately the same crystal structure. In the following, the effect of using pressure as a tuning parameter for  $\text{FePS}_3$  will be discussed.  $\text{FePS}_3$  was chosen because it is an antiferromagnetic insulator. It is also proposed to be a Mott insulator [5]. It has the lowest electrical band gap from the samples available in the group and previous work in the group has shown that it is most susceptible to pressure tuning.

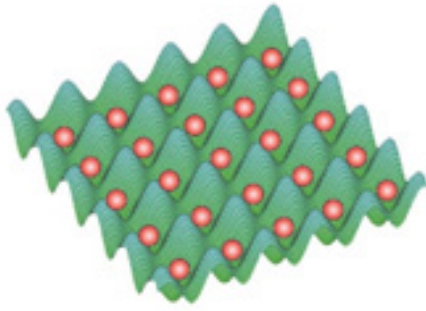


**Figure 2.2:** Graphic depiction of electrons (red) sitting in an atomic potential lattice (green) for a Mott insulator, where each site is occupied by one electron

exactly one electron) is depicted in figure 2.2. In the Hubbard model each electron is well localized at an atomic site and each site can contain at most two electrons (with opposite spin). The hamiltonian for this model is given by

$$\hat{H} = -t \sum_{i,j,\sigma} \hat{c}_{i\sigma}^\dagger \hat{c}_{j\sigma} + U \sum_i \hat{n}_{i\uparrow} \hat{n}_{i\downarrow} \quad (2.1)$$

where  $i, j$  are summed over neighbouring sites only, and  $s$  is the spinindex of the creation and annihilation operator ( $\hat{c}^\dagger, \hat{c}$  respectively). Furthermore  $\hat{n}_{i\sigma}$  is the number operator that indicates the number of electrons with

---

spin  $\sigma$  at site  $i$ .  $U$  and  $t$  can be found to express certain energies, because both quantities that are being summed over are dimensionless. The first term describes the hopping of electrons from one site to the next. The kinetic energy cost associated with this hopping is represented by  $t$ . The second term describes the number of atoms at a site  $i$  and  $U$  represents the Coulomb potential energy of two electrons sharing one such site.

When  $t \gg U$ , electrons are more likely to hop from one site to another and hardly feel the potential barriers separating the sites from one another. This has the effect that electrons can move freely through the lattice and the lattice therefore conducts electricity. This describes a metallic state.

If, however,  $U \gg t$ , the electrons are mostly confined to their atomic sites and don't hop from one site to another. This means the lattice doesn't conduct electricity and thus describes an insulating state. In this case an input of external (for example thermal) energy is needed in order for the electrons to hop between sites.

The magnitude of the parameters  $t, U$  are governed by the interatomic exchange interactions, which in turn are determined largely by the interatomic separation of the underlying lattice. By pressurizing a material, we can manipulate these separations and therefore tune these parameters from a  $U \gg t$  antiferromagnetic insulating state to a  $t \gg U$  metallic one. Chemical doping and other tuning methods can also be used, but in the following we will examine the influence of pressure on the crystal structure of  $FePS_3$  in order to understand more about the insulator to metal transition that was found to occur at high (order of GPa) pressures.

Crystallographic studies [7] have shown that in ambient conditions most materials from the  $MPX_3$  family (including  $FePS_3$ ) have a monoclinic unit cell from space group  $C2/m$ . An overview of  $FePS_3$ 's structural parameters is given in table 2.1. The crystal structure is given in figure 2.4. Fe atoms form 2D honeycomb lattices perpendicular to the c-direction. The P and S atoms form in strongly bonded  $P_2S_6$  clusters inbetween. These clusters of neighbouring layers are joined only by van der Waals forces, which allows for easy cleaving of the crystal in a-b planes. The magnetic moments of  $FePS_3$  point along the c-axis. The magnetic  $Fe^{2+}$  ions have spin  $S = 2$  and are Ising in character [8]. The material has a Neel temperature of 123K, below which the moments order ferromagnetically along the a-axis. These chains are in turn antiferromagnetically ordered with adjacent chains, giving rise to overall antiferromagnetism [8]. The magnetic structure of  $FePS_3$  is shown in figure 2.3.

All  $MPX_3$  materials are p-type semiconductors [5]. They exhibit extremely high room temperature resistivities and have band gaps in excess of 1eV [9]. As was mentioned before, previous work in the group showed

structural parameters	FePS <sub>3</sub>
a (Å)	5.947
b (Å)	10.30
c (Å)	6.722
$\alpha$	90°
$\beta$	107.2°
$\gamma$	90°

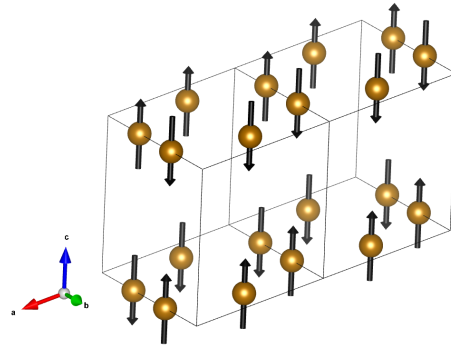


**Table 2.1:** Crystallographic data for FePS<sub>3</sub> (belonging to space group C2/m) from [7].

**Figure 2.3:** Magnetic Structure of FePS<sub>3</sub>. Ferromagnetically ordered chains along the a-direction can be seen to be ordered anti-ferromagnetically along the b and c-direction with neighbouring chains.

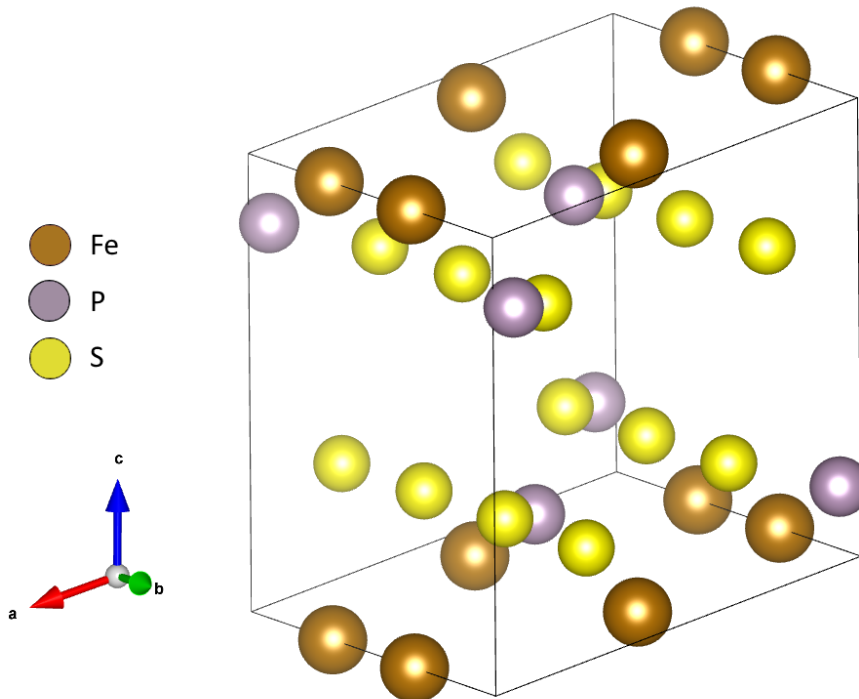


**Figure 2.4:** Crystal structure of FePS<sub>3</sub>. The iron layers are separated by two P<sub>2</sub>S<sub>6</sub> clusters that are bonded only via van-der-Waals forces. [8]

that  $FePS_3$  had the lowest resistivity and band gap. Many attempts have been made in theoretically calculating the band structure of  $FePS_3$  [5, 10], but none of them have yet been shown to reproduce the experimental data. Figure 2.5 shows the experimentally determined conductivity of  $FePS_3$  in the temperature range 250-500K by Grasso et al. in 1990. In order to extend this measurement to lower temperatures and examine the electric behaviour of  $FePS_3$  under pressure tuning, several measurements were made in the group.

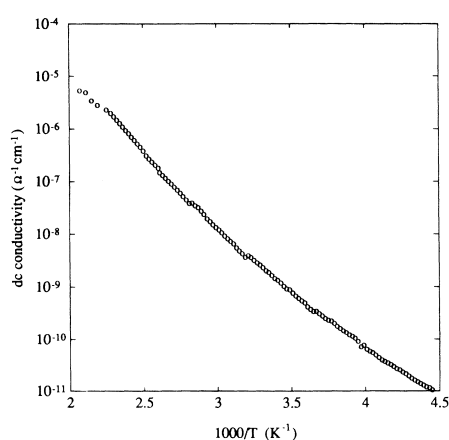


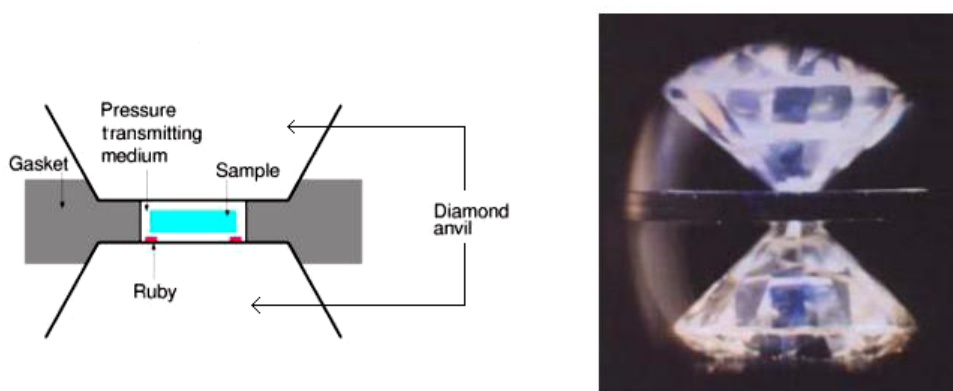
**Figure 2.5:** Temperature dependence of in-layer  $FePS_3$  DC conductivity. Adapted from [10]. Measurements of photoconductivity are omitted in this figure compared to the original.

Among other interesting results, that will be published in due time, these measurements confirmed the prediction that at high pressure  $FePS_3$  moves from an insulating to a metallic state. These results are depicted in figure 2.7 and figure 2.8. These measurements were obtained in tungsten carbide Bridgman anvil cells and pressures went up to 135kbar. Such a cell effectively puts the sample under pressure by applying force with two tungsten carbide anvils onto a gasket that contains the sample. An important aspect of Bridgman Anvil Cells is that the gasket also contains a powdered pressure medium. By using such a powder, higher pressures can be

obtained in Bridgman cells.

Unfortunately this medium also introduces a uniaxial strain across the sample, which is less than ideal because it effectively introduces a pressure gradient. The effect of the presence of this stress on the data depicted in figures 2.7 and 2.8 is still unclear.

For subsequent measurements Diamond Anvil Cells were used. Diamond Anvil Cells are effectively more refined Bridgman Anvil Cells, where the tungsten carbide anvil has been replaced by a sintered diamond anvil. They don't use a powder pressure medium and therefore don't introduce extra strain on the sample. A schematic overview of the workings of a Diamond Anvil Cell can be found in figure 2.6. An overview of the methodology in creating and using a Bridgman and Diamond Anvil Cell can be found in reference [11].



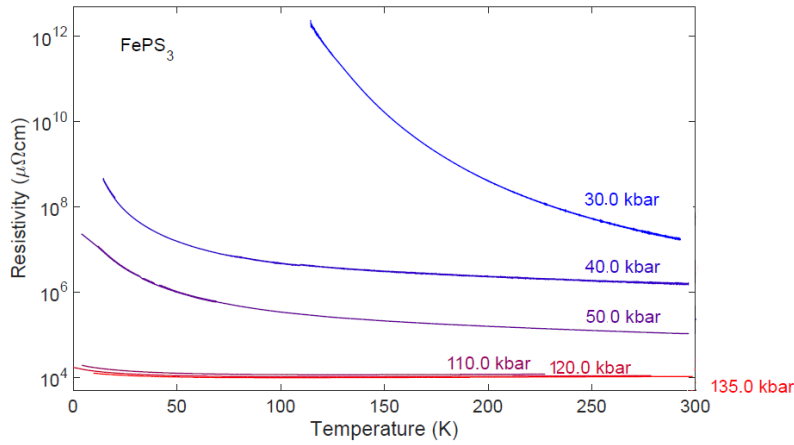
**Figure 2.6:** Left: Graphic depiction of the workings of a Diamond Anvil Cell. Right: photograph of the inner parts of a Cell.

Figure 2.7 shows all performed resistivity measurements at different pressures. Taking into account the logarithmic scale on the y-axis, it can be seen that the resistivity drops enormously with applied pressure. The actual sample resistances in these measurements in fact dropped from the range of  $G\Omega$  to the order of  $\Omega$ . When we look closer at the measurements at highest applied pressure (figure 2.8) we can also see a decreasing rather than increasing resistivity with temperature, giving further indication of a metallic state appearing at pressures over 100kbar.

In these results however, there is one other feature clearly visible. Whereas from room temperature downward the resistivity decreases with temperature, it starts to increase again around a temperature that itself seems to decrease with applied pressure. The increase of the resistivity at lower temperatures also seems to be repressed with higher applied pressure. The 120kbar data, which was obtained down to a temperature of about 100mK, additionally shows a gradual levelling off of this increase.

Previous attempts to fit the upturn into a seemingly metallic state with an Arrhenius or variable range hopping model as well as a dependence on the Kondo Effect have proven unsuccessful. Seeing as it can't be fitted to temperature dependencies of models describing known metallic behavior, we are likely dealing with some kind of exotic metallic state.

It was mentioned that the Bridgman anvil cells use a powder pressure medium in order to exert pressure on the sample. The benefit of using such cells with this medium is that they are able to obtain high enough pressures for the insulator-metal transition to occur as well as the fact that the pressure medium presses the contacts onto the sample. This means that the contact resistance in these cells will be negligible.



**Figure 2.7:** Resistivity of  $\text{FePS}_3$  as a function of temperature at several different estimated pressures ranging from 30 kbar to 135 kbar. Pressure was applied using a Bridgman Anvil Cell. Resistivity can be seen to be strongly suppressed via the application of pressure [11].

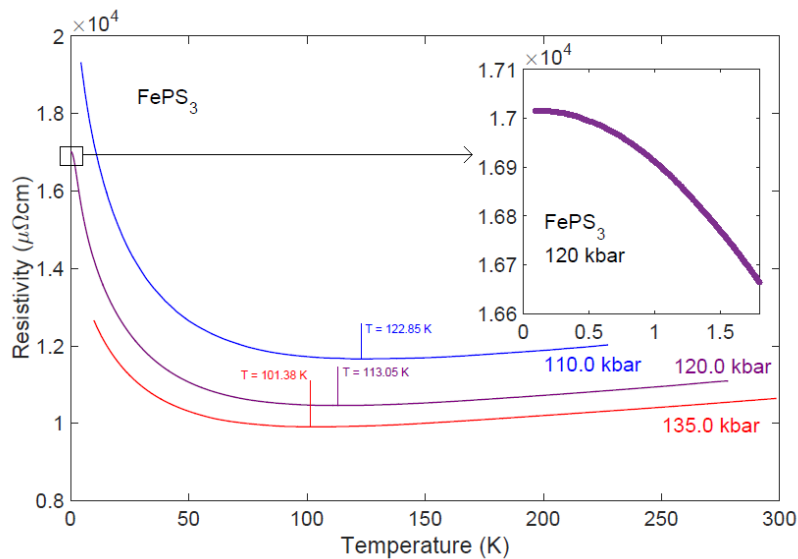


**Figure 2.8:** Resistivity of  $\text{FePS}_3$  as a function of temperature at several different estimated pressures ranging from 110 kbar to 135 kbar. Pressure was applied using a Bridgman Anvil Cell. Inset shows a levelling off of the upturn in resistivity in the low-temperature range of the data obtained at 120 kbar [11].

The downside, however, is that these cells invariably introduce a uniaxial stress on the sample. For the measurements depicted above this stress is exerted perpendicular to the crystal planes along the *c*-axis of the FePS<sub>3</sub>. This stress introduces a pressure gradient that is estimated to be about 20%. The weak inter-plane bonding of FePS<sub>3</sub> might enhance this effect even more.

In order to obtain more information about the strange insulator-metal transition described above, crystallography data at high pressure was subsequently obtained. Diamond Anvil Cells were used to obtain the necessary pressures. As was mentioned before, unlike Bridgeman cells, diamond anvil cells don't introduce a uniaxial strain across the sample. In ref [11] it is described how the problem of relatively poor contact resistance for diamond anvil cells at high pressures was overcome, using gold sputter-coating.

Two different powder X-ray diffraction datasets were obtained for pressures up to 180 and 310 kbar. In the first dataset no pressure medium was used, whereas for the second helium acted as the pressure medium. The introduction of helium as pressure medium generally leads to sharper and clearer peaks in the diffraction patterns. The downside to using helium as pressure medium at high pressures, however, is that from around 12GPa (or 120kbar) extra diffraction peaks appear. By examining the raw 2D diffraction data, it can be seen that these seem to have a significant preferred crystal orientation. This effect might be due to the solidification of helium under these pressures. These peaks were masked out in the data that is presented in this thesis. The full analysis of the data that was obtained with helium as a pressure medium is at the time of writing still underway.

The powder X-ray diffraction datasets were obtained at the Diamond Light Source Synchrotron in Oxford. Performing an X-ray diffraction measurement in a large synchrotron allows for obtaining much higher quality data than in most other setups. The XRD measurement gives a 2D diffraction pattern. Noise and diffraction peaks that originate from elements in the cell other than the sample, such as the diamond anvils in a DAC, have to be removed. The 2D diffraction pattern is then reduced to a 1D diffraction pattern via azimuthal integration, giving a more reliable overview of the diffraction data. This was done using Diamond's self-written software DAWN.

The data that was obtained without a gaseous pressure medium has been fully analyzed and will be discussed first. The 1D diffraction data was analyzed using the well-known method of Rietvelt refinement. Rietvelt refinement is basically a multi-parameter curve fitting procedure

---

[12]. It takes both the obtained diffraction Bragg peaks as well as a smooth background into account. Its results contrive, among others, of all relevant crystal structure parameters such as lattice parameters and atomic coordinates. Especially the lattice parameters are obtained with high precision.

In ref [7] it was shown that  $FePS_3$  has a monoclinic  $C2/m$  structure at ambient pressure. After the Rietveld fitting of the obtained diffraction data it was found that with the application of pressure this structure changes smoothly until it reaches a modified monoclinic  $C2/m$  structure at 10.1 GPa. The biggest difference between this state and the ambient pressure state is that  $\beta$  has changed from about  $107^\circ$  to  $90^\circ$ . This change in crystal structure is depicted in figure 2.9, which shows the view down the b and c-axis. The shift of the angle  $\beta$  can be seen from the shift in relative orientation of the iron atoms and is indicated by the grey lines connecting them in the view down the b-axis.

At even higher pressures another structural transition was found. The main aspect of this transition is a collapse of the interlayer spacing along the c-axis. This transition causes the structure to change from monoclinic  $C2/m$  to the closely related trigonal P-31m point space group. In this phase the iron atoms form perfect hexagons. The crystal structure of this high pressure phase is also depicted in figure 2.9. The collapse along the c-axis can be deduced from the changing structure parameters indicated below the visualizations of the view down the b-axis.

In figure 2.10 we see the Rietveld fits of the obtained data at ambient pressure, 10.1GPa and 18.1GPa. The last two can be considered as the 'endpoints' of the first and second structural transition. The data fits nicely with the crystal structures mentioned above. From the restricted fits we can obtain a quantitative analysis of the weight percentages of each structure throughout the transition. The associated weight factors of the intermediate  $C2/m$  and the final P-31m structure are depicted in figure 2.11. The midpoint of the first transition is at 3.6GPa. The midpoint of the second transition can be seen to lie around 13.7GPa. It should be mentioned that the original 2D diffraction data showed a significant preferred orientation, possibly because the  $FePS_3$  wasn't powderised enough. To account for this the fits used spherical harmonics.

Also, a discrepancy between the ambient pressure fit and the data at low ( $P < 2\text{GPa}$ ) pressures was found. The fit for the ambient pressure structure doesn't fit well with the data at these pressures. This might indicate that there is a new phase transition occurring at pressures below 1GPa. Because much is as of yet unclear about this, the transition at 3.6GPa will for now still be referred to as the 'first phase transition'.

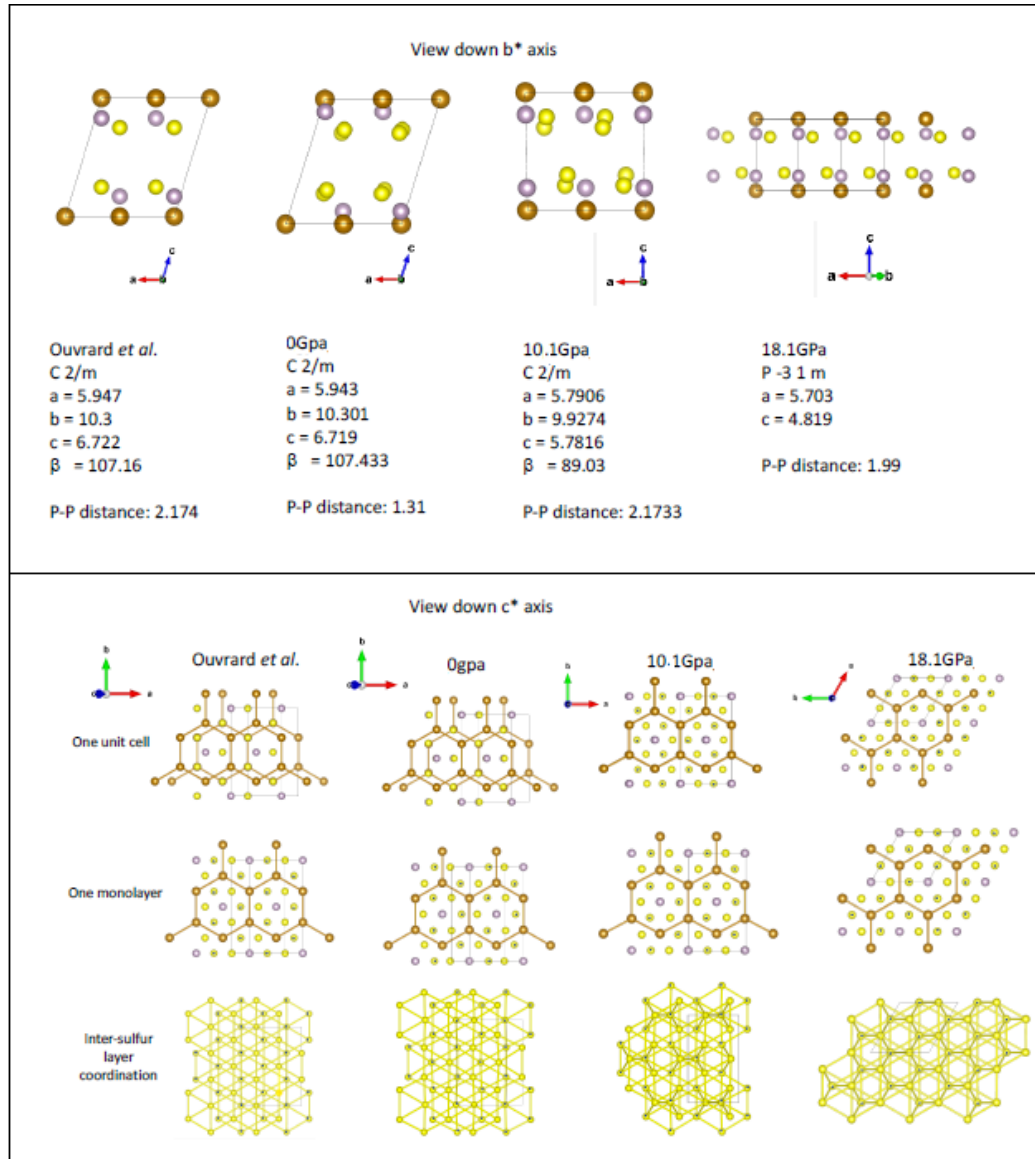


**Figure 2.9:** Proposed high-pressure crystal structures for FePS<sub>3</sub> after comparison with Rietvelt fits shown in figure 2.10. Ambient pressure structure is compared to proposed structure by Ouvrard *et al.* in ref [7]

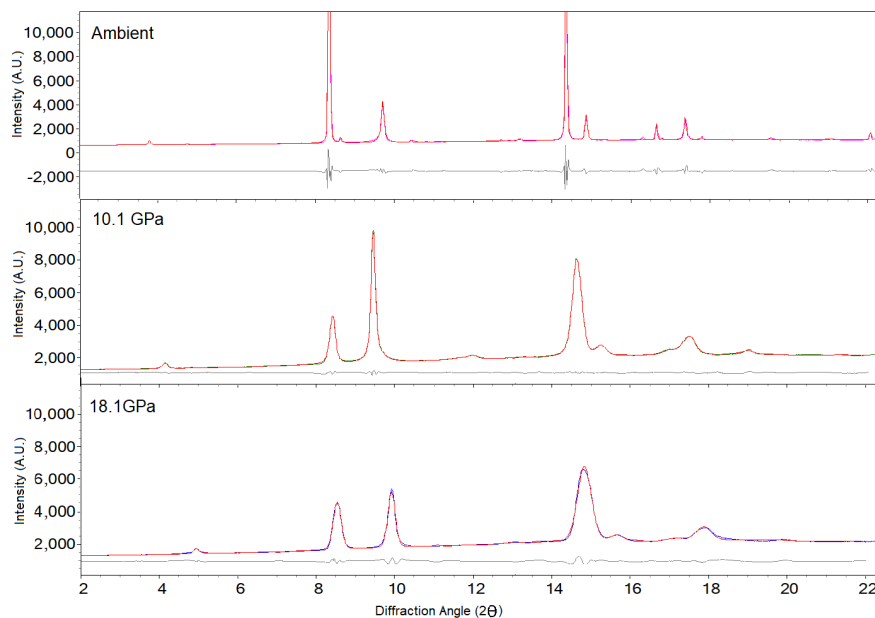


**Figure 2.10:** Obtained diffraction data for  $\text{FePS}_3$  at pressures of 0, 10.1 and 18.1 GPa. Diamond Anvil Cells without pressure medium were used. Obtained data is displayed in red and the relevant Rietveld fits for the proposed structures  $C2/m$ , modified  $C2/m$  and  $P-31m$  for the pressures 0, 10.1 and 18.1 are displayed in pink, green and blue respectively. The deviation of the obtained data from the Rietveld fit is displayed in gray below each dataset.

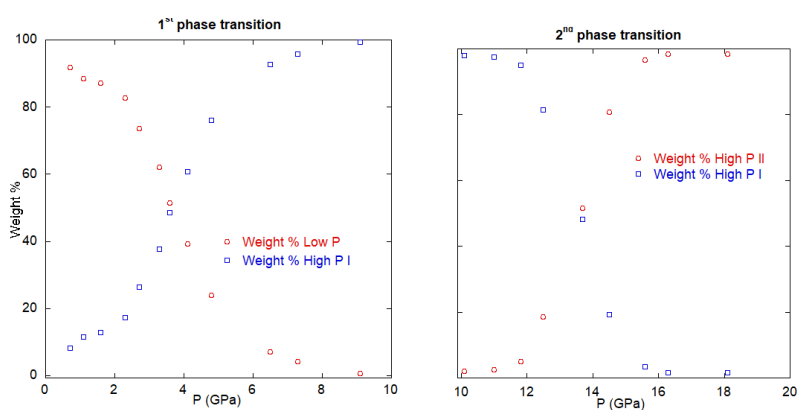


**Figure 2.11:** Refined weight percentages of the structural phases through the two crystal structure transitions in  $\text{FePS}_3$

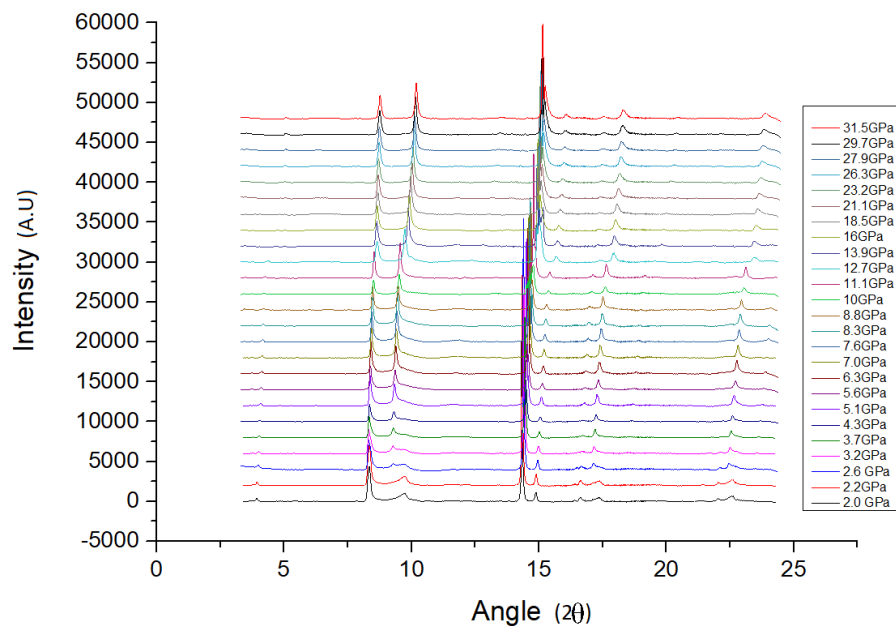


**Figure 2.12:** X-ray diffraction data for FePS<sub>3</sub> pressurized in a diamond anvil cell up till a pressure of 31.5GPa. Two transitions can be seen to occur around 2GPa and 12GPa. The intensity of the diffraction pattern is depicted in arbitrary units.

In order to obtain more insight into the problematic fits throughout the first transition, X-ray powder diffraction data was obtained at high pressures in a diamond anvil cell using helium as pressure medium. For this data less corrections for (anisotropic) peak broadening need to be considered, because it generally amounts to sharper diffraction peaks. The data was obtained up till pressures of 31.5GPa and is depicted in figure 2.12. Upon close scrutiny we can make out the two transitions. The first transition seems to occur over the pressure range 2-3GPa, where we can see - among other features - a peak around  $2\theta = 9^\circ$  disappearing and another at  $2\theta = 8^\circ$  reappearing.

The second transition occurs inbetween 11.1GPa and 12.7GPa. Here we see all diffraction peaks shift slightly to the right. This unilateral shift corresponds to the collapse of the c-axis.

In comparison to the earlier obtained diffraction data where no pressure medium was used, it can be seen that the obtained diffraction peaks are significantly sharper. This effect is especially noticable at higher pressures. The FWHM is approximately two times less for the diffraction peak at  $2\theta = 15^\circ$  around 18GPa for the helium data compared to the no-medium data. The Rietvelt analysis of the data presented above still has to be com-

pleted at the time of writing. This will however will most likely produce a much more detailed look into the change of crystal structure, because less (anisotropic) peak-broadening has to be taken into account in the analysis. Upon first inspection the structural transitions seem to occur at slightly different pressures for the latter dataset. Rietvelt refinement will shed more light on this possible discrepancy as well.

The exact relation between the structural crystallographic transitions mentioned above and the exotic metallic state of  $FePS_3$  under pressure is as of yet not understood. The added strain on the  $FePS_3$  samples during the resistivity measurements - due to the fact that a Bridgman anvil cell was used - might be of significant importance. This is why it would be useful to perform resistivity measurements down to low temperatures on  $FePS_3$  pressurised in diamond anvil cells. A comparison between these measurements and the diffraction data would be more straightforward.



## Pyrrhotite

Pyrrhotite is a strong carrier of magnetic remanence in both terrestrial and extra-terrestrial rocks. Therefore it effectively locks-in information about the direction and magnitude of the earth's magnetic field at the time the pyrrhotite was formed. This is why it has been extensively used over the last 50 years for purposes ranging from the documentation and determination of tectonic motions to the mapping of the secular variation in the earth's magnetic dipole moment [13]. Its presence in extra-terrestrial (among which Martian) meteorites, might also offer us a record of the history of the magnetic fields of the bodies that these originate from [14–17].

The full Pyrrhotite group is defined as the group of all iron monosulphides with an NiAs-type structure that possess the general formula  $Fe_{1-x}S$  where  $0 \leq x \leq 0.125$  represents the degree of iron deficiency [18]. These iron deficiencies can occur periodically in several different configurations, constituting so-called 'superstructures'. In pyrrhotite the superstructures are characterized by the periodicity of these vacancies in the direction of

the c-axis, where the c-axis is chosen to be orthogonal to the hexagonally structured Fe/S layers. Two superstructures that will be mentioned in the following are the monoclinic 4C superstructure, which has an effective monoclinic unit cell of 8 layers due to its ordered vacancies and the 5C\* superstructure, which has an effective unit cell of 10 layers with 4C chemical

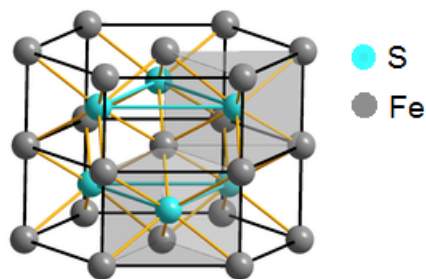


**Figure 3.1:** Structure of the unit cell of Pyrrhotite

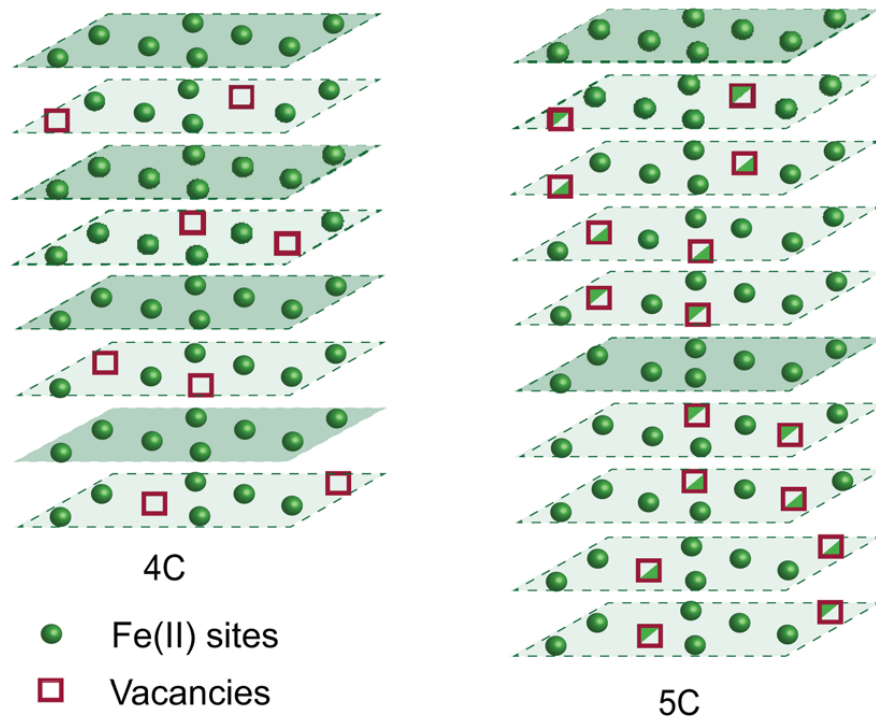


**Figure 3.2:** Schematic depiction of the location of the iron-deficiencies in pyrrhotite for superstructures of the form 4C (periodic in 8 layers) and 5C (periodic in 10 layers). Sulfur atoms are omitted for clarity. [19]

composition (see figure 3.2). The crystal structure of pyrrhotite is depicted in figure 3.1.

In the hexagonally structured basal plane, the moments of the iron atoms couple ferromagnetically and the adjacent iron-layers couple antiferromagnetically. The ordered array of iron vacancies gives rise to ferrimagnetism in monoclinic 4C pyrrhotite, which has an ideal formula of  $Fe_7S_8$ . The associated Curie temperature is  $350^\circ\text{C}$  and this phenomenon is well understood. However, at around 30K the magnetic and electric properties (among others) of this monoclinic pyrrhotite undergo a significant change, known as the Besnus transition [20]. This transition is characteristic for pyrrhotite and has been used for decades to identify the presence of this mineral in rock samples [13, 20].

The origin and mechanism of the Besnus transition has been disputed for decades. Ever since the (re)discovery of this transition by Fillion and Rochette [21], a mechanism similar to the Verwey transition in magnetite has been assumed. In essence, a Verwey transition is a simultaneous tran-

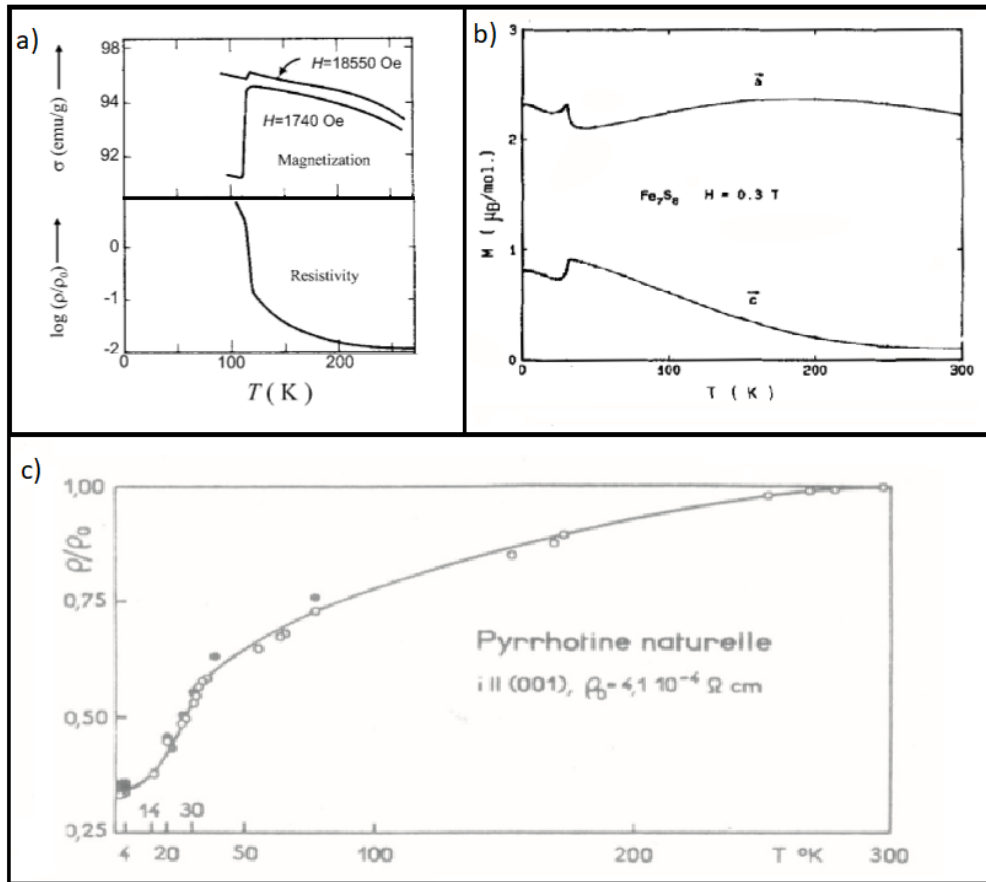


**Figure 3.3:** Summary of the earliest obtained magnetisation and resistivity data for Magnetite and Pyrrhotite. a) Top: magnetisation as a function of temperature for Magnetite. Around 120K a sudden drop in magnetisation, corresponding to the Verwey transition, can be seen. Below: a measurement of resistivity throughout the same transition [26, 27]. b) Magnetisation curves for pyrrhotite. The Besnus transition can be seen around 35K [21]. c) Resistivity curve for pyrrhotite where the Besnus transition manifests itself as a drop in resistivity around 35K [28].

sition of both the crystal lattice symmetry and the electrical and magnetic properties of a material. These kinds of abrupt changes of the crystallographic structure are usually accompanied by related anomalies in other control parameters, such as the specific heat [22]. A clear correspondence can be seen when we compare previously measured anomalies in monoclinic pyrrhotite to those of the Verwey transition in Magnetite (see figure 3.3). The exact mechanism, however, behind the Besnus transition is as of yet unclear and is still debated in the literature [18, 19, 23–25].

The question that this debate focuses on is whether or not the Besnus

transition is – in analogy with the Verwey transition – of crystallographic origin, meaning that it is explicitly intrinsic and material-specific, or whether it is magnetic in origin and stems from magnetic coupling of multiple superstructures associated with different iron vacancy distributions.

In support of the former interpretation Wolfers et al [25] performed a neutron diffraction study together with obtaining magnetic torque data for natural pyrrhotite to propose a monoclinic to triclinic crystallographic transition. This view is supported by the work of Volk et al [18], who showed a clear change from sixfold to fourfold magnetic anisotropy in the easy magnetization plane through the Besnus transition of a single crystal of monoclinic pyrrhotite.

Koulialias [19] and Charilaou [23], however, point out that in the paper by Wolfers et al, commensurate monoclinic pyrrhotite is assumed and the effect of heterogeneities is neglected. Furthermore, there have been neutron diffraction studies [24] and magnetic and spectroscopic studies [29] that support the absence of a crystallographic transition around 30K for synthetic single crystal and natural poly-crystalline pyrrhotite respectively.

Koulialias and Charilaou show instead, that magnetic coupling between the 4C superstructure and other structural inhomogeneities might be the underlying principle governing the Besnus transition. To support their claim, they offer powder X-ray diffraction data in combination with Rietveld refinement to show that their natural sample consists of a 4C superstructure in combination with a less pronounced 5C\* superstructure. The presence of this extra 5C\* structure above 35K was verified with hysteresis measurements of the easy-plane magnetization as a function of applied magnetic field. Hysteresis measurements at lower temperatures indicated that the anisotropy properties of the 5C\* structure might be embedded into those of the 4C structure after the Besnus transition, which was further evidenced by the appearance of a 12-fold symmetry in the magnetic resistivity below 30K. This would indicate strong coupling of these superstructures that form a unitary magnetic anisotropic system at the transition. This is why Koulialias and Charilaou claim that the Besnus transition is not related to an abrupt crystallographic transition, but that it is an extrinsic magnetic phenomenon that stems from the coupling between the dominant 4C superstructure of monoclinic pyrrhotite and other structural inhomogeneities.

In order to try to settle the debate about the origin of the Besnus transition, several different types of measurements have been performed in the group. Specific heat and magnetic measurements have been performed on two natural oriented pyrrhotite samples. Resistivity measurements were

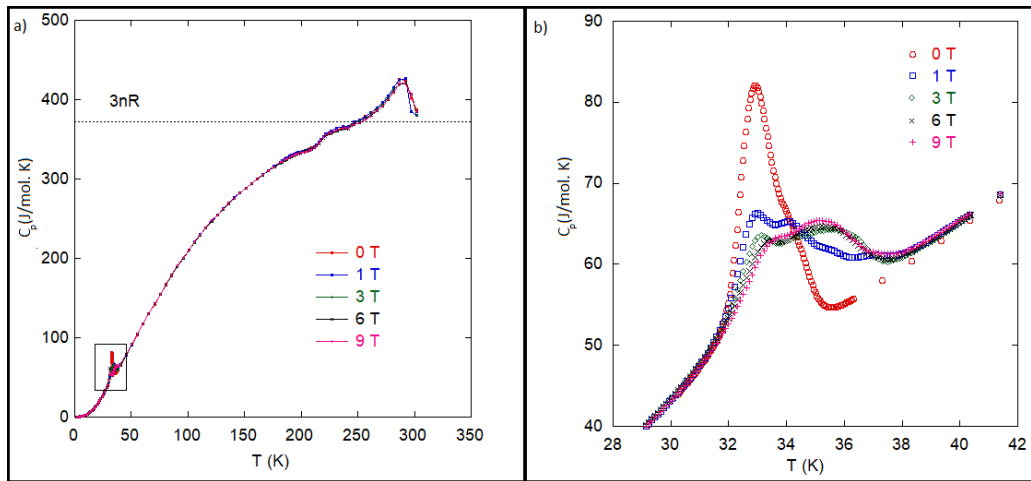


**Figure 3.4:** Results of measurements of specific heat of a single-crystal pyrrhotite sample as a function of temperature and magnetic field. An anomaly corresponding to the Besnus transition can be seen around 34K. Figure b) highlights the dual nature of this anomaly, consisting of two separate peaks: a broader magnetic field-dependent peak centered around 35K and a sharp - seemingly - field independent peak at 33K.

subsequently carried out in three orthogonal crystallographic directions in order to further investigate strong anisotropic effects in magnetization. Diffraction measurements indicated that the two samples that have been measured are samples of almost 'pure' 4C pyrrhotite  $Fe_7S_8(x \cong 0.125)$ . This means that for the measurements that will be discussed in the following, the effect of other types of structural inhomogeneities can seemingly be neglected.

Firstly, a Quantum Design PPMS was used to perform heat capacity measurements on a single crystal 'pure' 4C pyrrhotite sample under the application of magnetic fields of different strengths. The results are depicted in figure 3.4a. A clear anomaly related to the Besnus transition can be seen around 34K. When we take a closer look at the data around the transition it is clear that the anomaly in specific heat is field-dependent, decreasing in size with the application of a large magnetic field.

The resolution of the performed measurement allows us to distinguish not one, but two clear features that constitute the transition together. Instead of a single peak, the anomaly actually seems to be a linear superposition of two peaks centered around 35K and 33K. The 35K peak is broader and can often be seen as a shoulder to the much sharper peak around 33K. Moreover, the 35K peak shifts towards slightly higher temperatures

as the magnetic field is increased, whereas the 33K peak remains at approximately the same temperature (even though it decreases in size). This indicates that possibly it is only the temperature of the 35K anomaly that is field-dependent. As far as is known to the group, the dual nature of the transition as well as the difference in field-dependency has not been noted in the literature until now. In the rest of this thesis, as was the case before, the combination of these two anomalies will be referred to as ‘the Besnus transition’ as a whole.

Magnetisation was measured with a Quantum Design MPMS, in order to further investigate the magnetic properties of the Besnus transition. Firstly, the sample was cooled without applying a magnetic field (zero-field cooling) down to 2K. After this the magnetisation in the direction of the three principal crystallographic axes was measured upon heat-up under application of a 10mT field. The results of this measurement are depicted in figure 3.5a. A clear anisotropy can be seen in the magnetisation. At room temperature the direction of the overall magnetic moment is clearly in-plane ( $M \approx 0$  along the interlayer c-axis). However, from around 220K the magnetic moment along the c-axis gradually increases, whereas the in-plane components slightly decrease. The total

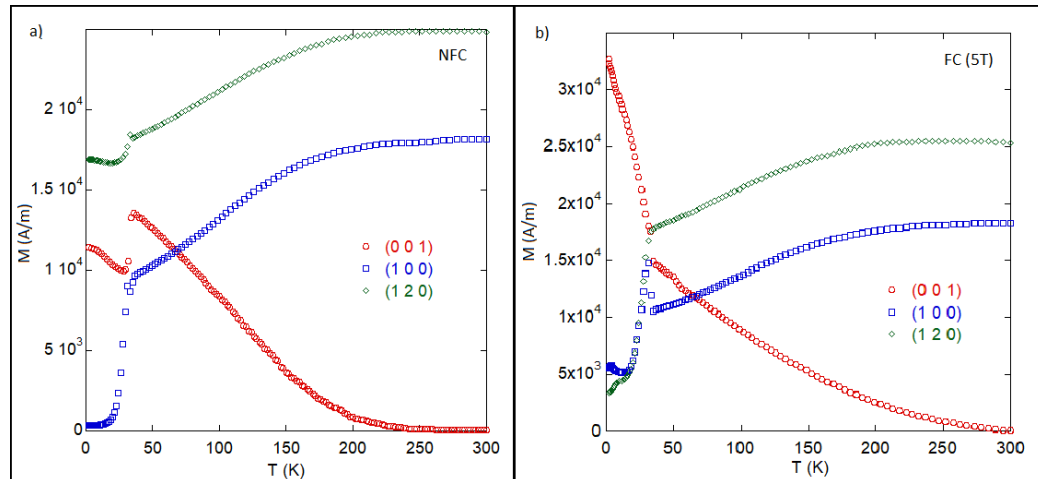


**Figure 3.5:** Zero-field cooled (a) and field cooled (b) magnetisation data of a single-crystal pyrrhotite sample with an applied magnetic field upon heating of 10mT. The magnetic moment is clearly anisotropic at all temperatures. The anomaly associated with the Besnus transition can be seen around 34K. Low-temperature behavior depends strongly on the application of a magnetic field upon cooling, indicating the importance of magnetic domain formation after the Besnus transition.

---

magnetic moment stays the same, which indicates that the magnetic moments slowly rotate out of the plane when the sample is cooled from room temperature down to the Besnus transition. At the Besnus transition there is a sudden drop in magnetisation along all principal axes. This drop leads to an overall decrease in total magnetic moment. This drop suggests a possible formation of local magnetic domains partly cancelling each other.

This assertion has been tested by cooling the sample from room temperature down to 2K under the application of a magnetic field of 5T (field-cooling). Field-cooling saturates the magnetisation along the direction of the applied magnetic field. This means that forming of possibly opposing magnetic domains will be prevented. When the applied magnetic field is then removed at base-temperature and the magnetisation is measured upon heating it can be seen that the total magnetic moment is conserved (see figure 3.5), contrary to the zero-field cooled results. This means that the Besnus transition is nothing more than a reordering of the same magnetic moments that are present at room temperature.

In order to further investigate the anisotropic effects governing the transition, 4-point electrical resistivity measurements were made for two oriented natural pyrrhotite samples in three orthogonal crystallographic directions characterized by the miller indices (100),(120) – both in-plane – and (001) which is along the c-axis.

Resistivity measurements were performed using a Princeton Applied Research 5210 and an EG&G 7265 Lock-in Amplifier in combination with a current supplier of  $500\mu\text{A}/\text{V}$ . The lock-ins operated at a frequency of 1115Hz with an oscillation voltage of 2V. Both were chosen in order to reduce noise from an unknown source with frequency peaks at multiples of 10 and 15Hz. This noise remained constant when the oscillation voltage was increased. This is why the highest possible setting (2V) was chosen in order to improve the S/N-ratio as much as possible. Most of the presented data is scaled, however, to the resistivity at 280K or 33K (transition temperature) which eliminates the effect of the noise-filters that were used. When the magnitude of the resistivity is concerned, artificial noise filtering has been corrected for. Furthermore, measurements of different samples (of the same chemical composition) along the same crystallographic direction with two different lock-ins indicated that the effect of using different lock-ins as well as the effect of performing the measurements on different samples from the same batch can be neglected.

For each measurement  $25\mu\text{m}$  gold wires were spot-welded to the sample surface in a Kelvin 4-probe configuration along each of the previously mentioned crystallographic directions. The connections were subsequently enforced by applying 4929 DuPont highly conductive air dry epoxy. The

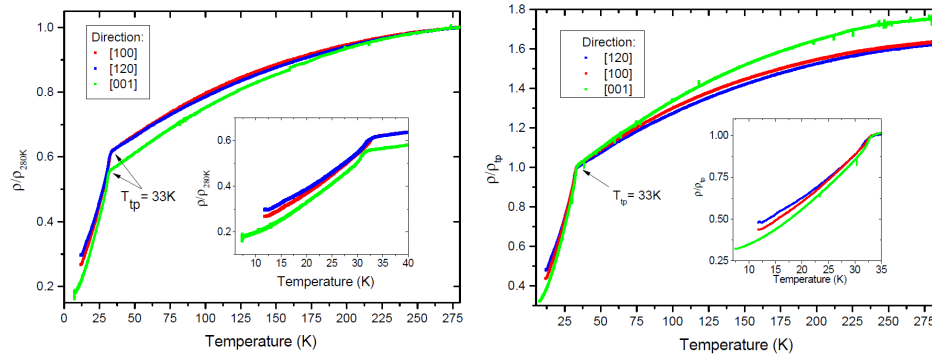


**Figure 3.6:** Resistivity measurements along three orthogonal crystallographic directions scaled to their resistivity at a) 280K and b) 33K (transition point)

samples were cooled down using a Cryomech PT407 Pulse Tube Refrigerator in combination with a Cryomech CP970 helium compressor. Without thermal load this system will go down to a temperature of 2.8K [30] but because of the relatively large thermal load of our setup as well as possible contaminations of the  $^4He$  gas used, the actual measurements went down to about 7.5K. A Lakeshore 370 AC Resistance Bridge was used in order to obtain accurate temperature control. The exact pressure was not recorded, but turbo pump vacuum is assumed.

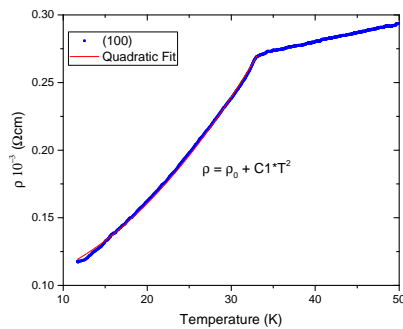


**Figure 3.7:** Quadratic fit of temperature range 10-35K of the resistivity curve for pyrrhotite down to 10K in the (100) direction.

to settle at a residual resistivity between  $0.10 - 0.15 \cdot 10^{-3} \Omega cm$ . In addition a residual resistance ratio of around 1/4 was found. Both values are

An overview of the resistivity measurements can be found in figure 3.6. Anisotropy in the conductivity is apparent, although not as pronounced as one might expect from the previously presented magnetization data. In the temperature-regime below the besnus transition magnetic scattering dominates the resistivity of the material. This can be deduced from the  $T^2$  fit in figure 3.7 corresponding to  $e - e$  scattering as a dominant mechanism in increasing the resistivity with increasing temperature. When the magnitude is concerned, the resistivity curve seems

lower, by a small margin, than what has previously been reported in the literature. This thus further indicates the lack of structural defects in the samples used.

In order to further confirm the dual nature of the transition the derivative of the resistivity with respect to temperature is plotted in figure 3.8. Because the determination of this dual nature requires data of high resolution, no smoothing algorithm was used in processing the data. The dual nature of the transition can be seen in the local maximum of the derivative around 34K. When the pyrrhotite is heated up through the transition the derivative first starts to increase around 30K. This increase reaches a local maximum around 32K after which it starts to decrease and settle to an approximately constant value at 34K. These temperatures are somewhat lower than the interval for the transition obtained during the magnetisation/specific heat measurements. Even though the samples were cut from the same batch as the ones that were used for those measurements, the discrepancy might be an effect of the usage of different samples. A further possibility might be that the effect in resistivity is only a characteristic of the lower-temperature transition. This would then mean that the magnetic field dependent higher temperature transition would have no effect on the resistivity of pyrrhotite. More detailed measurements and analyses in the future might offer more insight into the viability of these possibilities.

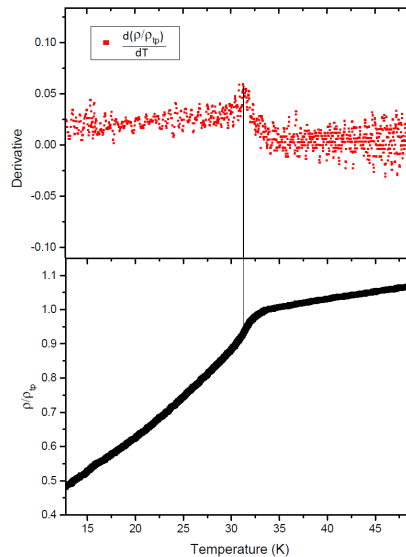


**Figure 3.8:** Derivative of resistivity around the Besus transition. When temperature is increased through the transition, the derivative can be seen to first rise in the interval 30-32K and after this settle down to a value lower than before the transition. No smoothing algorithm was used in order to keep the resolution as high as possible.



## Summary & Outlook

In this thesis research is presented into two types of exotic anti ferromagnets, namely  $FePS_3$  and  $Fe_{1-x}S$  (pyrrhotite). As of yet unexplained behavior has been described and possible models describing the magnetic and crystallographic structure of these materials are proposed. X-ray diffraction, resistivity, magnetization and specific heat measurements have been performed and these have led to the crystallographic structural and magnetic models that are proposed for  $FePS_3$  and pyrrhotite respectively.

Resistivity measurements show the emergence of an unconventional low-temperature metallic state in  $FePS_3$  when pressures exceeding 100kbar are applied. The temperature dependency of the resistivity could not be fitted to any of the theoretical models known (to the group), which is why subsequently X-ray diffraction measurements were obtained. From these diffraction measurements two structural transitions can be ascertained, with the possibility of a third low-pressure ( $P < 10\text{kbar}$ ) transition. The analysis of the subsequently obtained diffraction data of  $FePS_3$  pressurized in Diamond Anvil Cells with helium as a pressure medium might offer better resolution of this structural analysis, seeing as data that is obtained this way is generally sharper and goes up to higher pressures.

An important fact that is noted is that the resistivity measurements were performed in Bridgman Anvil Cells, which inherently introduce a uniaxial strain and thus a pressure gradient on the sample that is estimated to be about 20%. In the diffraction measurements Diamond Anvil Cells were used that don't introduce this strain, which means that two different kinds of physics might apply for these situations. In order to further investigate the effect of the added strain it will be useful to perform resistivity measurements down to cryogenic temperatures on samples that have been pressurized in Diamond Anvil Cells. Comparison of the resis-

tivity data with the data obtained in Bridgman Anvil Cells will then possibly offer both a qualitative and a quantitative measure of the effect of the added pressure gradient on the found exotic metallic low-temperature state.

Specific heat, magnetization and resistivity measurements were performed on pyrrhotite, with the specific focus on anisotropy during the 'Besnus transition'. This transition is characterized by a sudden drop in resistivity around 30-36K together with jumps in the magnetization and a specific heat anomaly. The mechanism governing this transition has been heavily debated in the literature with the focus being on whether the transition is a structural crystallographic transition (much like the Verwey transition in magnetite) or whether the transition comes about from the interplay of multiple magnetic superstructures. The results presented in this thesis provide compelling evidence for the exclusion of the latter interpretation. Even though no definitive conclusion can be made at this time, this research does point to the importance of the magnetic domain structure of pyrrhotite involved in the Besnus transition. This is why further exploration with the means of low-temperature neutron diffraction studies might offer more insight into the change in magnetic structure in this 30-36K temperature range.

Furthermore, the detailed and high resolution measurements that are presented in this thesis seem to evidence the existence of two separate transitions, together constituting a phenomenon that has traditionally been described as a single transition. This observation is of significant importance and can't be omitted in any discussion regarding the Besnus transition. As far as it is known in this group, the dual nature of this transition has never been noted before in the literature.

## Acknowledgements

A lot of people have contributed knowingly and unknowingly to what has been presented in this thesis. Below is a list of people that wouldn't and shouldn't be surprised to find their name here:

- David Jarvis
- Matthew Coak
- Sebastian Haines
- Siddharth Saxena
- All other members of 'the group'

*The aim of this research was to understand and make brighter that what we know. This has been the case during writing and hopefully reading as well. In any case, the results are exciting and speak for themselves. Because, as is known to the writer, results will go up when temperatures go low.*



# Bibliography

- [1] M. R. Norman, *The Challenge of Unconventional Superconductivity*, Science **332**, 196 (2011).
- [2] Guest Editors and Laura H Greene and Joe Thompson and Jörg Schmalian, *Strongly correlated electron systems - reports on the progress of the field*, Reports on Progress in Physics **80**, 030401 (2017).
- [3] N. P. Armitage, P. Fournier, and R. L. Greene, *Progress and perspectives on electron-doped cuprates*, Rev. Mod. Phys. **82**, 2421 (2010).
- [4] P. Monthoux and G. G. Lonzarich, *Magnetically mediated superconductivity: Crossover from cubic to tetragonal lattice*, Phys. Rev. B **66**, 224504 (2002).
- [5] V. Grasso and L. Silipigni, *Low-Dimensional Materials: The MPX3 Family - Physical Features and Potential Future Applications*, Cheminform **34** (2003).
- [6] J. C. Slater and G. F. Koster, *Simplified LCAO Method for the Periodic Potential Problem*, Phys. Rev. **94**, 1498 (1954).
- [7] G. Ouvrard, R. Brec, and J. Rouxel, *Structural determination of some MPS3 layered phases (M = Mn, Fe, Co, Ni and Cd)*, Materials Research Bulletin **20**, 1181 (1985).
- [8] D. Lancon, H. C. Walker, E. Ressouche, B. Ouladdiaf, K. C. Rule, G. J. McIntyre, T. J. Hicks, H. M. RÅžnnow, and A. R. Wildes, *Magnetic structure and magnon dynamics of the quasi-two-dimensional antiferromagnet FePS3*, Physical Review B **94**, 11. 214407 (2016).

- 
- [9] K.-z. Du, X.-z. Wang, Y. Liu, P. Hu, M. I. B. Utama, C. K. Gan, Q. Xiong, and C. Kloc, *Weak Van der Waals Stacking, Wide-Range Band Gap, and Raman Study on Ultrathin Layers of Metal Phosphorus Trichalcogenides*, *ACS Nano* **10**, 1738 (2016).
- [10] V. Grasso, F. Neri, S. Patančič, L. Silipigni, and M. Piacentini, *Conduction processes in the layered semiconductor compound  $\text{FePS}_3$* , *Phys. Rev. B* **42**, 1690 (1990).
- [11] M. Coak, *Quantum Tuning and Emergent Phases in Charge and Spin Ordered Materials*, PhD dissertation, University of Cambridge, Cambridge, 2017.
- [12] R. B. V. Dreele, *Protein Crystal Structure Analysis from High-Resolution X-Ray Powder-Diffraction Data*, in *Macromolecular Crystallography, Part C*, volume 368 of *Methods in Enzymology*, pages 254 – 267, Academic Press, 2003.
- [13] *Paleomagnetism of the Notch Peak contact metamorphic aureole, revisited: Pyrrhotite from magnetite+pyrite under submetamorphic conditions*, **108** (2003).
- [14] Louzada Karin L., Stewart Sarah T., and Weiss Benjamin P., *Effect of shock on the magnetic properties of pyrrhotite, the Martian crust, and meteorites*, *Geophysical Research Letters* **34** (2007).
- [15] Hood L. L., Richmond N. C., Pierazzo E., and Rochette P., *Distribution of crustal magnetic fields on Mars: Shock effects of basin-forming impacts*, *Geophysical Research Letters* **30** (2003).
- [16] P. Rochette, G. Fillion, R. Ballou, F. Brunet, B. Ouladdiaf, and L. Hood, *High pressure magnetic transition in pyrrhotite and impact demagnetization on Mars*, *Geophysical Research Letters* **30**.
- [17] P. ROCHETTE, J. GATTACCECA, V. CHEVRIER, V. HOFFMANN, J. LORAND, M. FUNAKI, and R. HOCHLEITNER, *Matching Martian crustal magnetization and magnetic properties of Martian meteorites*, *Meteoritics & Planetary Science* **40**, 529.
- [18] M. W. Volk, S. A. Gilder, and J. M. Feinberg, *Low-temperature magnetic properties of monoclinic pyrrhotite with particular relevance to the Besnus transition*, *Geophysical Journal International* **207**, 1783 (2016).
-

- [19] D. Koulialias, J. Kind, M. Charilaou, P. Weidler, J. Löffler, and A. Gehring, *Variable defect structures cause the magnetic low-temperature transition in natural monoclinic pyrrhotite*, *Geophysical Journal International* **204**, 961 (2016).
- [20] Rochette Pierre, Hood Lon, Fillion Gerard, Ballou Rafik, and Ouladdiaf Bachir, *Impact demagnetization by phase transition on Mars*, *Eos, Transactions American Geophysical Union* **84**, 561 (2011).
- [21] G. Fillion and P. Rochette, *The low temperature transition in monoclinic pyrrhotite*, <http://dx.doi.org/10.1051/jphyscol:19888412> **49** (1988).
- [22] F. Walz, *The Verwey transition - a topical review*, *Journal of Physics: Condensed Matter* **14**, R285 (2002).
- [23] M. Charilaou, J. Kind, D. Koulialias, P. G. Weidler, C. Mensing, J. F. Löffler, and A. U. Gehring, *Magneto-electronic coupling in modulated defect-structures of natural Fe<sub>1-x</sub>S*, *Journal of Applied Physics* **118**, 083903 (2015).
- [24] A. V. Powell, P. Vaqueiro, K. S. Knight, L. C. Chapon, and R. D. Sánchez, *Structure and magnetism in synthetic pyrrhotite Fe<sub>7</sub>S<sub>8</sub>: A powder neutron-diffraction study*, *Phys. Rev. B* **70**, 014415 (2004).
- [25] P. Wolfers, G. Fillion, B. Ouladdiaf, R. Ballou, and P. Rochette, *The Pyrrhotite 32 K Magnetic Transition*, *Solid State Phenomena* **170**, 174 (2011).
- [26] P. Weiss and R. Forrer, *La saturation absolue des ferromagnetiques et les lois d'approche en fonction du champ et de la temperature*, *Annales des Physique* **10**, 279 (1929).
- [27] T. Okamura, *Scientific Reports of Tohoku University* **1**, 231.
- [28] M. Besnus and A. Meyer, *Nouvelle donnees experimentales sur le magnetisme de la pyrrhotine naturelle*, in *Proc. Int. Conf. Mag.*, pages 507–511, Nottingham, 1964.
- [29] J. Kind, I. García-Rubio, M. Charilaou, N. R. Nowaczyk, J. F. Löffler, and A. U. Gehring, *Domain-wall dynamics in 4C pyrrhotite at low temperature*, *Geophysical Journal International* **195**, 192 (2013).
- [30] Cryomech, *Cryorefrigerator Specification Sheet - PT407 with CP970*, 2012.